Unveiling growth histories of multi-generational garnet in a single skarn deposit via newly-developed LA-ICP-MS U Pb dating of grandite

Article *in* Gondwana Research · September 2019

DOI: 10.1016/j.gr.2019.04.003

CITATIONS
2

READS
328

7 authors, including:

Shitao Zhang
Chinese Academy of Sciences
11 PUBLICATIONS **36** CITATIONS
SEE PROFILE

Yu Zhang
Central South University
41 PUBLICATIONS **125** CITATIONS
SEE PROFILE

Gaobin Chu
Guangzhou institute of geochemistry, China academy of science
7 PUBLICATIONS **7** CITATIONS
SEE PROFILE

Gondwana Research 73 (2019) 65–76

Contents lists available at ScienceDirect

Gondwana Research

journal homepage: www.elsevier.com/locate/gr

Unveiling growth histories of multi-generational garnet in a single skarn deposit via newly-developed LA-ICP-MS U—Pb dating of grandite

Shitao Zhang [a,b], Huayong Chen [a,c,*], Qihai Shu [d], Yu Zhang [e], Gaobin Chu [a,b], Jiamin Cheng [a,b], Jing Tian [a,b]

[a] CAS Key Laboratory of Mineralogy and Metallogeny, Guangzhou Institute of Geochemistry, Chinese Academy of Sciences, Guangzhou 510640, China
[b] University of Chinese Academy of Sciences, Beijing 100049, China
[c] Guangdong Provincial Key Laboratory of Mineral Physics and Materials, Guangzhou 510640, China
[d] State Key Laboratory of Geological Processes and Mineral Resources, School of Earth Sciences and Resources, China University of Geosciences, Beijing 100083, China
[e] Key Laboratory of Metallogenic Prediction of Nonferrous Metals and Geological Environment Monitor, Central South University, Changsha 410083, China

ARTICLE INFO

Article history:
Received 2 February 2019
Received in revised form 29 March 2019
Accepted 7 April 2019
Available online 26 April 2019

Keywords:
Grandite LA-ICP-MS U—Pb dating
U concentration
Skarn hydrothermal events
Tonglvshan Cu-Fe-Au deposit

ABSTRACT

Although garnet U—Pb dating method has been reported recently, yet the accurate concordia $^{206}Pb/^{238}U$ ages and growth histories of multi generation of garnets based on ages were still lacked. LA-ICP-MS U—Pb dating on multi-generational grandite (grossular-andradite) garnet from the large Tonglvshan Cu-Fe-Au skarn deposit was applied in this study. Based on petrographic observation, in chronological order, three generation garnets have been distinguished, namely homogeneous Grt1-exo (in the exoskarn zone) and Grt1-endo (in the endoskarn zone), oscillatory zoning Grt2 and vein-type Grt3 cutting magnetite ores. LA-ICP-MS U—Pb dating on four grandite samples from the Grt1-exo, Grt1-edno, Grt2 and Grt3 yields Tera-Wasserburg lower intercept $^{206}Pb/^{238}U$ ages of 139.1 ± 1.0 Ma (2σ, MSWD = 0.79), 134 ± 11 Ma (2σ, MSWD = 2.5), 143.4 ± 8.3 Ma (2σ, MSWD = 2.3) and 140.3 ± 1.4 Ma (2σ, MSWD = 0.95), respectively. More importantly, two concordia $^{206}Pb/^{238}U$ ages of 139.2 ± 0.6 Ma (2σ, MSWD = 1.4) and 139.8 ± 1.5 Ma (2σ, MSWD = 0.13) were firstly obtained from the sample of Grt1-exo with highest U concentrations ($[U]_{avg}$ > 80 ppm) contents. The precision U—Pb ages of 139–140 Ma from Grt1-exo and Grt3 can be considered as the timing of Cu-Fe-Au skarn mineralization, and consistent with the majority of published zircon U—Pb ages of the quartz dioritic stock and $^{40}Ar—^{39}Ar$ plateau ages of phlogopite at Tonglvshan (142–140 Ma). The precision grandite U—Pb ages also indicate that the entire metasomatic hydrothermal mineralization activity in the Tonglvshan Cu-Fe-Au skarn deposit occurred within a relatively short time span of <1 (or 2.5 considering errors) Myr. In addition, we found that the grandite garnet is more easily to be enriched in U and can obtain the high-precision concordia U—Pb ages with higher andradite Mol%, euhedral and larger crystals, and relevant oxidized magmatic rocks or skarns.

1. Introduction

In the past decades, multiple isotopic dating methods have been applied to constrain the timing of worldwide skarn mineralization, such as U—Pb dating of magmatic- and hydrothermal zircon (Chiaradia et al., 2009; Deng et al., 2015a; Zhao et al., 2016), titanite (Li et al., 2010; Deng et al., 2015b) and cassiterite (Yuan et al., 2011; Zhang et al., 2017a); Re—Os isotopic dating of molybdenite (Xie et al., 2011; Li et al., 2018c) and $^{40}Ar—^{39}Ar$ geochronology of phlogopite and hornblende (Cheng et al., 2013; Li et al., 2014).

In spite of this, in many cases, due to lacking of suitable dating minerals, the timing of skarn and relevant ore formation cannot be directly constrained, and only referenced to the crystallization ages of assumed causative intrusive rocks or late dikes (Nokleberg, 1981; Gevedon et al., 2018). Whereas in other instances, due to the lack of spatially related intrusive rocks in the mining area, the ore-forming age and genesis of the deposit have caused great controversy (Tornos et al., 2000; Fang et al., 2018; Zhang et al., 2018b). Moreover, on the mineral scale, it was hardly to determine the growth rates and histories of skarn minerals, needless to say the duration and longevity of skarn hydrothermal mineralization process (e.g., Meinert et al., 2005).

Garnet, especially grandite (grossular ($Ca_3Al_2Si_3O_{12}$) to andradite ($Ca_3Fe_2Si_3O_{12}$)), is a ubiquitous mineral in the skarn systems (Grew et al., 2013; Deng et al., 2017). At present, melt/fluid inclusions, stable oxygen isotope and trace elements of garnet have been widely used to reconstruct the *P-T* evolution of skarn and related mineralization (e.g. Meinert et al., 2003; Chang and Meinert, 2008; Gaspar et al., 2008; Zhang et al., 2017b). Regarding geochronology, unlike the high-grade metamorphism, Lu—Hf and Sm—Nd isotopic dating

* Corresponding author at: CAS Key Laboratory of Mineralogy and Metallogeny, Guangzhou Institute of Geochemistry, Chinese Academy of Sciences, Guangzhou 510640, China.
E-mail address: huayongchen@gig.ac.cn (H. Chen).

https://doi.org/10.1016/j.gr.2019.04.003
1342-937X/

methods are scarcely used in the skarn systems, due to the commonly low Lu and Hf contents and variable Nd initial isotope ratios, respectively (Jamtveit and Hervig, 1994; Gaspar et al., 2008; Zhang et al., 2018b). Even so, garnet has a wide *P-T* stability, resistance to weathering and alteration, and high closure temperature for the U—Pb isotope system (>850 °C; Mezger et al., 1989), making it a potentially suitable geochronometer (Mezger et al., 1991; Burton et al., 1995). However, due to the low U contents and interference of mineral inclusions, garnet U—Pb isotopic dating was long been discarded by the traditional isotope dilution-thermal ionization mass spectrometry (ID-TIMS) (Seman et al., 2017; Salnikova et al., 2018). Lima et al. (2012) obtained an ID-TIMS U—Pb age (318.36 ± 0.32 Ma) of uranitite inclusions in garnet from a pegmatite vein in Évora, Portugal. But it is a pity that the precise U—Pb age cannot directly represent the formation age of garnet.

Recently, benefiting from the development of laser ablation inductively coupled plasma-mass spectrometry (LA-ICP-MS), several in-situ garnet U—Pb isotopic dating have been reported for some different types of skarn deposits (e.g., Deng et al., 2017; Seman et al., 2017). But most of them were influenced by the high common Pb contents, and failed to yield accurate concordant U—Pb ages with only the Tera-Wasserburg lower intercept $^{206}Pb/^{238}U$ ages and ^{207}Pb-corrected U—Pb ages obtained (Li et al., 2018a; Gevedon et al., 2018; Wafforn et al., 2018; Zhang et al., 2018b). In this contribution, we present LA-ICP-MS U—Pb isotope ages (including both concordia and lower intercept ages) and major and trace elements data for the multi-generational grandite garnets from the large Tonglvshan Cu-Fe-Au skarn deposit, eastern China and discuss the variation of U in garnet with their influences on U—Pb age constrains, and the timing and duration of hydrothermal mineralization process in a single skarn deposit.

2. Geological setting

The Middle-Lower Yangtze River metallogenic belt (hereafter referred to as the MLYRB), lying in the northeast to the Yangtze Craton and south to the North China Craton and Qinling-Dabie orogenic belt, is one of the vitally important Cu-Fe-Au skarn provinces in China, consisting of Edong, Jiurui, Anqing-Guichi, Tongling, Luzong, Ningwu and Ningzhen ore districts from west to east (Fig. 1a and b; Mao et al., 2011; Zhou et al., 2015). The Edong ore district located in the western of the MLYRB is well endowed with Cu-Fe-(Au), Fe-(Cu) and W-Cu-(Mo) skarn (-porphyry) deposits, and is one of the important Cu-polymetallic skarn districts in eastern China (ESM 1 Fig. 1; Li et al., 2014; Xie et al., 2015). The Cambrian to Middle Triassic marine carbonate and clastics are widespread with a thickness of >6 km (ESM 1 Fig. 1; Xie et al., 2015). The Late Mesozoic intermediate to felsic intrusions were extensively distributed in the Edong ore district with a total outcrop area of ~700 km^2 (ESM 1 Fig. 1; Li et al., 2014; Zhang et al., 2018a). Around these plutons, numerous skarn deposits have been found in the last several decades (ESM 1 Fig. 1). For example, Cu-Fe-(Au) and Fe—Cu skarn deposits spatially related to the Yangxin and Tieshan diorites, and Fe skarn deposits associated with the Echeng and Jinshandian granitoids (Xie et al., 2015).

The large-scale Tonglvshan Cu-Fe-Au skarn deposit (lat. 30°04′30″N, long. 114°55′42″ E) is located in the Edong ore district, MLYRB with proven metal reserves of 86.3 Mt. @ 1.66% Cu, 0.94 g/t Au and 39.4% Fe (Fig. 1c; ESM1 Fig. 1; Li et al., 2010; Zhang et al., 2018a). The exposed strata in the Tonglvshan mining area are the Lower Triassic Daye Formation mainly consisting of limestone and dolomite (Fig. 1c; Li et al., 2010). The quartz monzodiorite (porphyry) stock with an outcropped area of 11 km^2, intruded into the Lower Triassic carbonate rocks at 142–140 Ma (Xie et al., 2011; Li et al., 2014; Zhang et al., 2018a). The

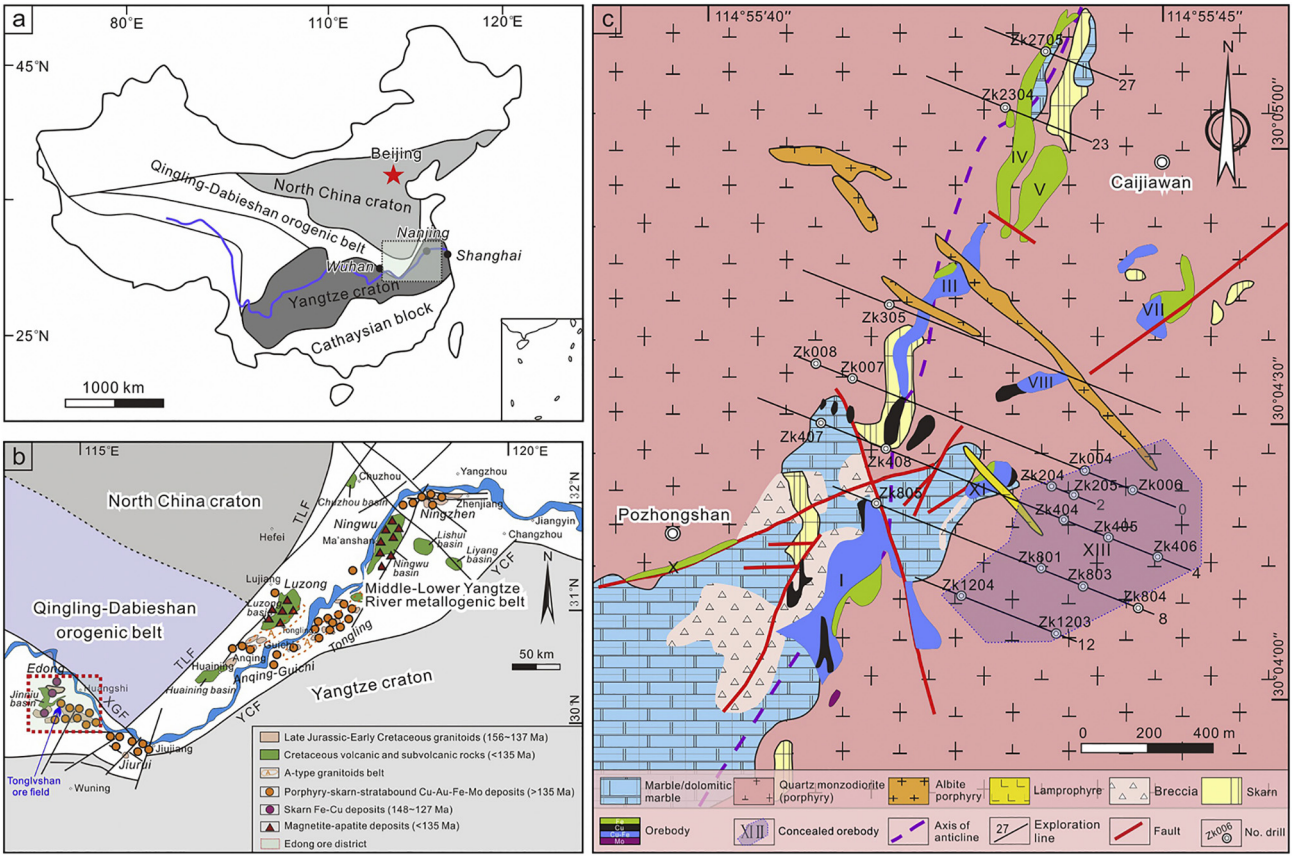

Fig. 1. (a) Simplified geological map of China; (b) Location of the Edong ore district in the Middle-Lower Yangtze River Valley metallogenic belt (modified after Mao et al., 2011 and Zhang et al., 2018b) (TLF: Tancheng-Lujiang fault; XGF: Xiangfan-Guangji fault; YCF: Yangxing-Changzhou fault). (c) Geological map of the Tonglvshan Cu-Fe-Au skarn deposit (modified after Li et al., 2010 and Zhang et al., 2018a).

quartz monzodiorite was widespread in the Tonglvshan mining area, while the quartz monzodiorite porphyry locally occurred in the internal contact zone in the deep area (Zhang et al., 2018a). Thirteen skarn Cu-Fe-Au orebodies, mainly occurring as lenticular and stratiform shape, have been discovered in the Tonglvshan ore deposit (Zhang et al., 2018a). They are mainly distributed along the NNE faults and the contact zone between the quartz monzodiorite/quartz monzodiorite porphyry and the marble/dolomitic marble (Fig. 1c).

At Tonglvshan, several distinct mineralization/alteration stages have been distinguished: pre-ore prograde skarn alteration (stage I, dominated by garnet, diopside, K-feldspar and wollastonite), retrograde alteration (stage II, featured by abundant epidote, actinolite, phlogopite, serpentine and magnetite) and oxide (stage III, dominated by hematite, specularite and quartz) with Fe mineralization, quartz-sulfide (stage IV, featuring by abundant chalcopyrite, bornite, chalcocite, pyrite and quartz) with Cu—Au mineralization, and post-ore carbonate (stage V, dominated by calcite and ankerite) and supergene process (stage VI, featured by malachite and azurite) (Zhang et al., 2018a).

3. Garnet petrography

Garnet was one of the most important alteration minerals in the Tonglvshan Cu-Fe-Au skarn deposit. Based on the mineral assemblages and their mega/microscopic texture relationships, three distinct generations of garnet have been identified with a youngling trend, namely homogeneous garnet in the exoskarn zone (Grt1-exo) and endoskarn zone (Grt1-endo) and oscillatory zoning garnet (Grt2) in the pre-ore prograde skarn stage (stage I), and garnet-calcite veins (Grt3) in the sulfide (stage IV) to carbonate (stage V) stages (Fig. 2).

Early Grt1-endo mainly occurs as veins or irregular grains with colors of light- to dark brown replacing quartz monzodiorite in the endoskarn zone (Fig. 2a, b). Under the BSE image, Grt1-endo shows nonuniform of chemical composition with residual plagioclase (Fig. 2b). In the exoskarn zone, almost simultaneous Grt1-exo usually presents as garnet-diopside or garnet skarn (Fig. 2c, d). The colors of Grt1-exo range from dark brown to bottle green in hand specimen (Fig. 2c, d). Under the plane-polarized light and BSE image, Grt1-exo commonly shows isotropic with some hematite micro veins cutting in late stage (Fig. 2e, f). The Grt2 usually grows along the crystal edges of Grt1-exo with light brown to light green in colors, and showing conspicuous oscillatory zoning texture (Fig. 2d, e, g). Under the plane-polarized light and BSE image, Grt2 shows distinct elemental zoning with late hematite micro veins cutting (Fig. 2g, h).

Retrograde alteration stage (stage II) of epidote and magnetite replacing Grt1 and Grt2 are commonly distributed at Tonglvshan deposit (Fig. 2i). Moreover, the garnet-calcite (Grt3) veins cutting massive magnetite ores with residual diopside also have been found (Fig. 2j, k). The Grt3 is relatively homogeneous with some previous magnetite and diopside inclusions (Fig. 2l). Although the precedence relationship between Grt3-calcite vein and quartz-sulfide ores (stage IV) was not observed at Tonglvshan, based on the existing metasomatism relationship, such as disseminated chalcopyrite and chalcopyrite-quartz vein replacing garnet-diopside skarn (Fig. 2c) and calcite replacing Grt2 (Fig. 2d, e), Grt3 probably grew in the sulfide (stage IV) to carbonate (stage V) stages, and can approximately represent the end of the main Cu-Fe-Au skarn mineralization event at Tonglvshan deposit.

4. Analytical methods

Thirteen samples of the three generational garnets (Grt1-endo, Grt1-exo, Grt2 and Grt3) at Tonglvshan for the scanning electron microscopy (SEM) and electron probe microprobe analysis (EMPA) were directly conducted on the polished thin section that cut from the hand specimens. Each garnet sample has been observed carefully under microscope and SEM to investigate their internal textures and mineral inclusions. Backscatter electron (BSE) images of garnet grains were taken by the Zeiss Supra 55 field emission SEM at the State Key Laboratory of Isotope Geochemistry, Guangzhou Institute of Geochemistry, Chinese Academy of Sciences (GIG-CAS). The chemical composition and major element mapping analyses of garnet were determined by using a JEOL JXA-8230 EMP at the Key Laboratory of Mineralogy and Metallogeny, GIG-CAS. The instrument was operated in wavelength-dispersion mode with a beam diameter of 1 μm, an accelerating voltage of 15 kV, and a probe current of 20 nA. Natural silicate minerals were used as standards, including rhodonite (Mn and Ca), pyrope (Mg, Al and Si), almandine (Fe), rutile (Ti), chromium oxide (Cr) and metallic nickel (Ni). Detection limits for the elements are below 0.01 wt%. All data were reduced using the ZAF correction program. Detailed instrument parameters and analytical procedure about the major element mapping analyses of garnet were given by Li et al. (2018b).

Four of the above 13 garnet samples (ZK803-97A, ZK2705-145, ZK803-97B and ZK204-56) were selected for in situ U—Pb isotopic dating and trace elements analyses. Moreover, another garnet sample (ZK804-75) from a garnet skarn in the exoskarn zone was selected for trace element mapping analyses. In situ garnet U—Pb isotopic dating and trace element and mapping analyses were performed by LA-ICP-MS at the Key Laboratory of Marine Resources and Coastal Engineering, Sun Yat-sen University. The laser sampling was performed using an ArF excimer laser ablation system (GeoLasPro), and ion-signal intensities were acquired using an Agilent 7700 × ICP-MS. A 44 and 60 μm laser spot was used with an energy density of 5 J/cm^2 and a repetition rate of 5 Hz. The trace element compositions of garnet were calibrated against the National Institute of Standards and Technology Standard Reference Material 610, using the Si determined by electron microprobe as the internal standard. Zircon 91,500 was used as the external standard to correct U—Pb isotopic ratios. Time-dependent drifts of U-Th-Pb isotopic ratios were corrected using a linear interpolation (with time) for every 10 analyses, based on the variations of Zircon 91,500. The final uncertainties were propagated from uncertainties of the preferred and measured Zircon 91,500 values, and from the measured sample values (Fu et al., 2015).

For comparison and monitoring the precision and accuracy of the U—Pb dating results, the samples of ZK803-97A and ZK204-56 were analyzed twice with ten month intervals using different secondary garnet standard (QC04 and WS20) and laser spot beam of 44 and 60 μm, respectively. Andradite garnet (QC04) was collected from the Qicun Fe skarn deposit in the Han-Xing district, North China Craton, China (Deng et al., 2017), and schorlomite garnet (WS20) was collected from a wollaston ite-ijolite at the Prairie Lake carbonatite complex, Northwestern Ontario, Canada (Yang et al., 2018). The obtained weighted mean $^{206}Pb/^{238}U$ ages of 128 ± 3 Ma (2σ; MSWD = 0.42; n = 8) and 1159 ± 6 Ma (2σ; MSWD = 0.60; n = 38) for QC04 and WS20, respectively, are consistent with the recommended values (QC04: 130 ± 2 Ma, Deng et al., 2017; WS20: ~1160 Ma, Yang et al., 2018; ESM2 Table 1). Each analysis consisted of 20 s of background measurement (laser-off) followed by 45 s of data acquisition. Data reduction was performed using ICPMSDataCal software (Liu et al., 2010). Isoplot 3.0 was used to calculate the U—Pb ages and weighted $^{206}Pb/^{238}U$ mean ages, and draw Tera-Wasserberg Concordia diagrams (Ludwig, 2003). Detailed instrument parameters and analytical procedure were given by Li et al. (2018a).

5. Results

5.1. Major element garnet geochemistry

The major elements of garnet at Tonglvshan Cu-Fe-Au skarn deposit are listed in appurtenant material (ESM 2 Table 1) and illustrated in Fig. 3. Electron microprobe analyses (EMPA) show that the three generation garnets at Tonglvshan all belong to the grossular-andradite (grandite) solid solution series and fall into the field of Cu- and Fe skarn deposits in the worldwide (Fig. 3; Meinert et al., 2005). The

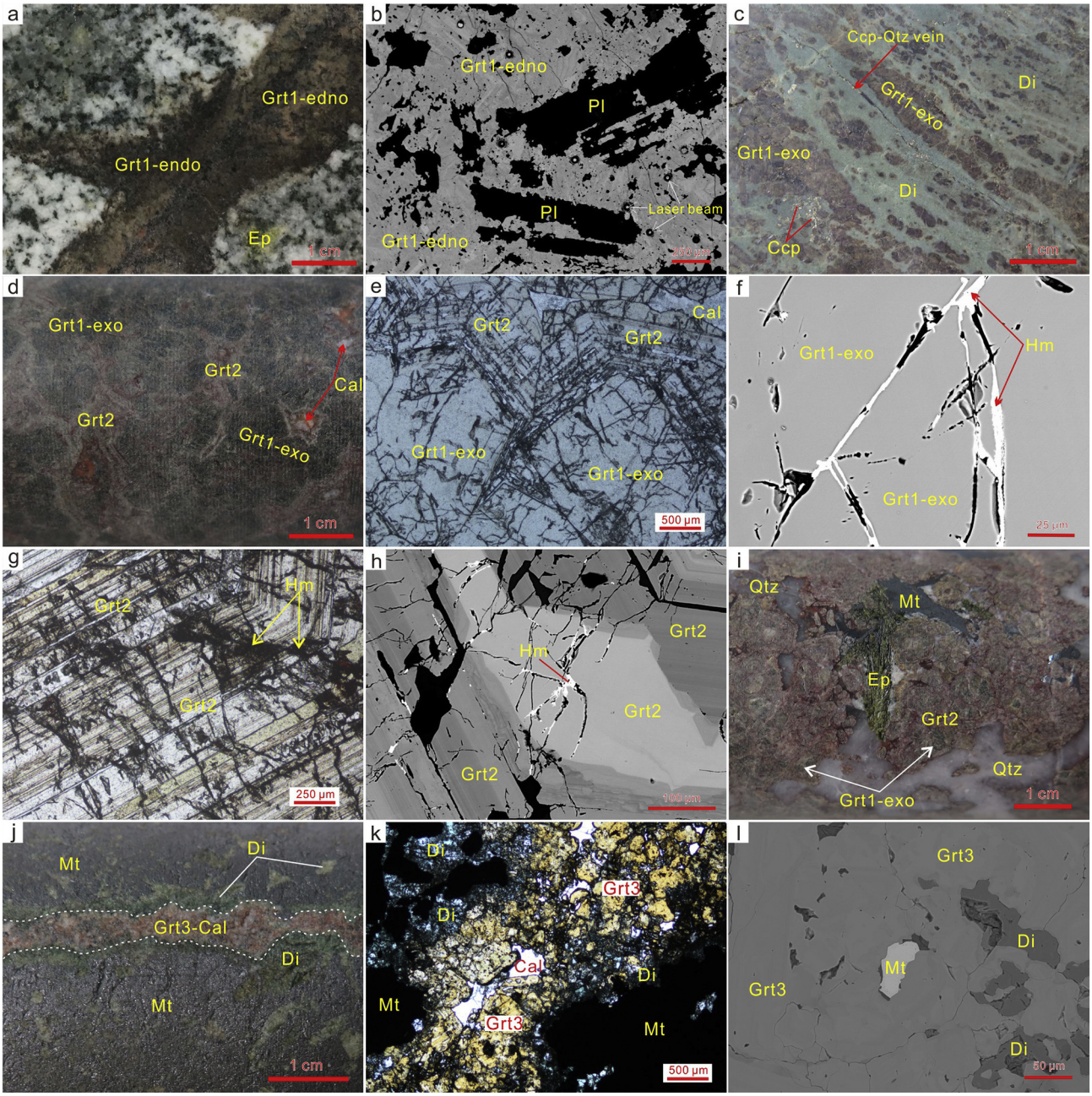

Fig. 2. Photographs and photomicrographs showing the different generation/ occurrences of garnet in the Tonglvshan Cu-Fe-Au skarn deposit. (a) Photograph showing brown garnet vein (Grt1-endo) cutting quartz monzodiorite with montmorillonite and epidote alteration; (b) Photomicrograph under BSE image showing Grt1-endo replacing plagioclase in the quartz monzodiorite; (c) Photograph showing garnet-diopside skarn (Grt1-exo) replaced by disseminated chalcopyrite and chalcopyrite-quartz vein; (d) Photograph showing the bottle green garnet (Grt1-exo) around by light brown to light green garnet (Grt2) that replaced by calcite in the late stage; (e) Photomicrograph under plane-polarized light showing homogeneous Grt1-exo around by zoning Grt2 and then replaced by the calcite in the late stage; (f) Photomicrograph under BSE image showing homogeneous Grt1 with hematite micro veins in the flaw; (g) Photomicrograph under plane-polarized light showing zoning Grt2 with a lots of flaws and filled by hematite; (h) Photomicrograph under plane-polarized light showing zoning Grt2 with a lots of flaws and filled by hematite; (i) Photograph showing the bottle-green garnet (Grt1-exo) and light green garnet (Grt2) replaced by magnetite-epidote-quartz; (j and k) Photograph and photomicrograph under plane-polarized light showing the garnet-calcite (Grt3) vein cutting massive magnetite ores with residual diopside; (l) Photomicrograph under BSE image showing some of diopside and maganetite inclusions in the Grt3. Abbreviations: Grt1-endo = the first generation of garnet in the endoskarn zone; Ep = epidote; Pl = plagioclase; Grt1-exo = the first generation of garnet in the exoskarn zone; Di = diopside; Ccp = chalcopyrite; Qtz = quartz; Grt2 = the second generation of garnet; Cal = Calcite; Hm = hematite; Mt. = magnetite; Grt3 = the third generation of garnet. (For interpretation of the references to color in this figure legend, the reader is referred to the web version of this article.)

composition of garnets range from $Adr_{18.4}Gro_{79.8}$ to almost pure andradite ($Adr_{99.8}Gro_{0.2}$) with almandine, pyrope, spessartine and uvarovitee collectively <3.5% (Fig. 3; ESM 2 Table 1). As the diversity of textural and microscopic features in petrography, the major element composition of garnets show large variations.

The first generation garnet (Grt1) in the exoskarn zone show obviously andradite-rich ($Adr_{>83.6}$), while in the endoskarn zone (i.e., proximity to the Tonglvshan quartz monzodiorite) range from $Adr_{40.5}Gro_{56.9}$ to $Adr_{78.0}Gro_{20.2}$ (ESM 2 Table 1). Oscillatory zoning garnets (Grt2) show large chemical oscillations with the composition range from $Adr_{18.4}Gro_{79.8}$ to almost pure andradite ($Adr_{99.8}Gro_{0.2}$) (Fig. 3; ESM 2 Table 1). The major elements mapping by EMPA show that Grt2 has Al-rich cores and Fe-rich rims with distinct oscillatory zonal of Al and Fe (Fig. 4a), but Fe-rich cores and Al-rich rims can also be found

(Fig. 4b). The elements of Mn, Ti and Mg show slightly enriched in the core of Grt2 (Fig. 4). In addition, the composition of Grt3 from garnet-calcite veins range from $Adr_{53.7}Gro_{45.4}$ to $Adr_{80.9}Gro_{16.9}$ (Fig. 3; ESM 2 Table 1).

5.2. Trace element garnet geochemistry

Trace elements of the Tonglvshan garnet are listed in ESM 3 Table 2 and illustrated in Fig. 5. On the whole, the REE concentrations (110–1637 ppm) have large variations in different occurrence/generation garnets, but generally display LREE enrichment and HREE depletion and positive Eu anomalies (Fig. 5; ESM 3 Table 2). The total REE of Grt1 in the endoskarn zone range from 151 to 959 ppm with average values of 325 ppm. Uranium and Th contents range from 4.2 to 26.2 ppm and 1.8 to 38.3 ppm, respectively, with Th/U ratios of 0.4–3.0 (ESM 3 Table 2). While, for the Grt1 in the exoskarn zone, the total REE range from 274 to 606 ppm with average values of 477 ppm (Fig. 5a; ESM 3 Table 2). Notably, it has higher U contents with average values of 82 ppm (ESM 3 Table 2). This is an ideal sample for in-situ garnet U—Pb dating.

Compared to the isotropic Grt1 in the exoskarn zone, the total REE of zoning Grt2 (110–264 ppm) show significantly decreased with average values of 148 ppm. Moreover, there are lower U contents with average values of 16 ppm in Grt2 (ESM 3 Table 2). For Grt3, the total REE range from 243 to 1637 ppm with average value of 755 ppm (ESM 3 Table 2). It is obviously higher than other generation garnets. The last generation of Grt3 has variable U contents with values range from 9.1 to 102 ppm (ESM 3 Table 2).

5.3. Garnet U—Pb geochronology

Garnet U—Pb isotopic data are listed in ESM 4 Table 3 and illustrated in Fig. 6. The sample of ZK803-97A (Grt1-exo) has high U contents ($[U]_{avg}$ > 80 ppm) and has been analyzed twice. For the first time, a total of 38 analyses with laser spot of 60 μm yielded a Tera-Wasserburg diagram with lower intercept $^{206}Pb/^{238}U$ age of 139.1 ± 1.0 Ma (MSWD = 0.79) (Fig. 6a) and the selected 23 analyses yielded a concordia $^{206}Pb/^{238}U$ age of 139.2 ± 0.6 Ma (MSWD = 1.4) (Fig. 6b). For the same sample, ten months later in the same lab, twenty-six analyses with a smaller laser spot (~ 44 μm) yielded a lower intercept $^{206}Pb/^{238}U$ age of 139.8 ± 2.6 Ma (MSWD = 0.48) (Fig. 6c) and the selected 15 analyses yielded a concordia $^{206}Pb/^{238}U$ age of 139.8 ± 1.5 Ma (MSWD = 0.13) (Fig. 6d). In comparison, the Grt1-endo sample ZK2705-145B has low U ($[U]_{avg}$ = 12 ppm) and produced a lower intercept $^{206}Pb/^{238}U$ age of 134 ± 11 Ma (MSWD = 2.5; n = 33) (Fig. 6e).

The sample of ZK803-97B (Grt2) also has low U contents ($[U]_{avg}$ = 16 ppm). A total of 31 analyses yielded a Tera-Wasserburg diagram with lower intercept $^{206}Pb/^{238}U$ age of 143.4 ± 8.3 Ma (MSWD = 2.3) (Fig. 6f). In addition, twice analysis for the sample ZK204-56 (Grt3) with elevated U concentration ($[U]_{avg}$ ≥ 35 ppm) yielded lower intercept $^{206}Pb/^{238}U$ ages of 140.3 ± 1.4 Ma (MSWD = 0.95; n = 39) (Fig. 6g) and 141.0 ± 3.3 Ma (MSWD = 1.1; n = 38) (Fig. 6h), respectively.

6. Discussion

6.1. The incorporation of U into grandite garnet

Sufficient U concentrations and negligible common Pb contents in the crystal lattice of mineral are necessary conditions for U—Pb isotopic dating (Mezger et al., 1989; Deng et al., 2017). Uranium-rich mineral inclusions, such as zircon, monazite, uraninite and allanite often occur in the garnet, and can severely influence the results of direct U—Pb dating of garnet (Dewolf et al., 1996; Lima et al., 2012). However, recently, several published grandite garnets in the skarn system are lack of this phenomenon (Deng et al., 2017; Gevedon et al., 2018; Zhang et al., 2018b). In this study, we found that grandite garnet in the Tonglvshan Cu-Fe-Au skarn deposit have large variations of U (4–131 ppm) (ESM 4 Table 3). Under the BSE images, only some later tiny cracks and filled hematite can be observed in Grt1 and Grt2; while in the Grt3, minor magnetite and diopside inclusions, rather than U-rich mineral inclusions occurred (Fig. 2f, h, l), suggesting that U possibly occurs within the grandite garnet lattice. Moreover, the time-resolved signals of Si, U, Th, Pb and LREEs

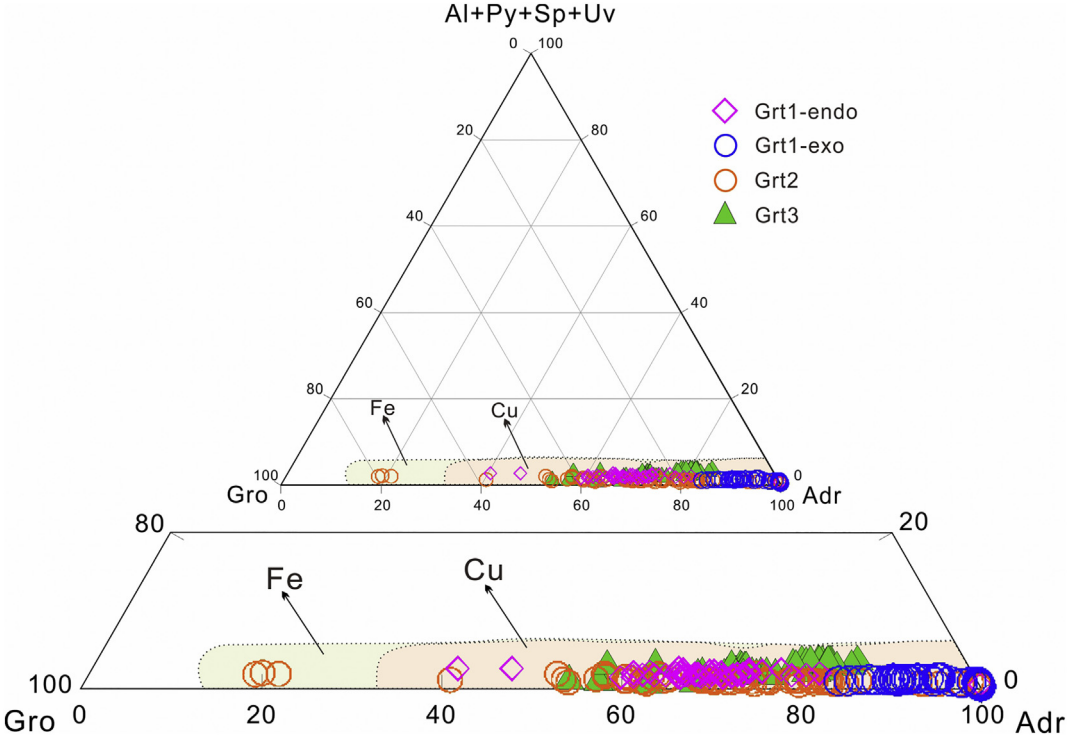

Fig. 3. Triangular classification of garnet in the Tonglvshan Cu-Fe-Au deposit (the base map according to Meinert et al., 2005). Abbreviations: Adr = andradite; Gro = grossular; Al = almandine; Py = pyrope; Sp = spessartine; Uv = uvarovite.

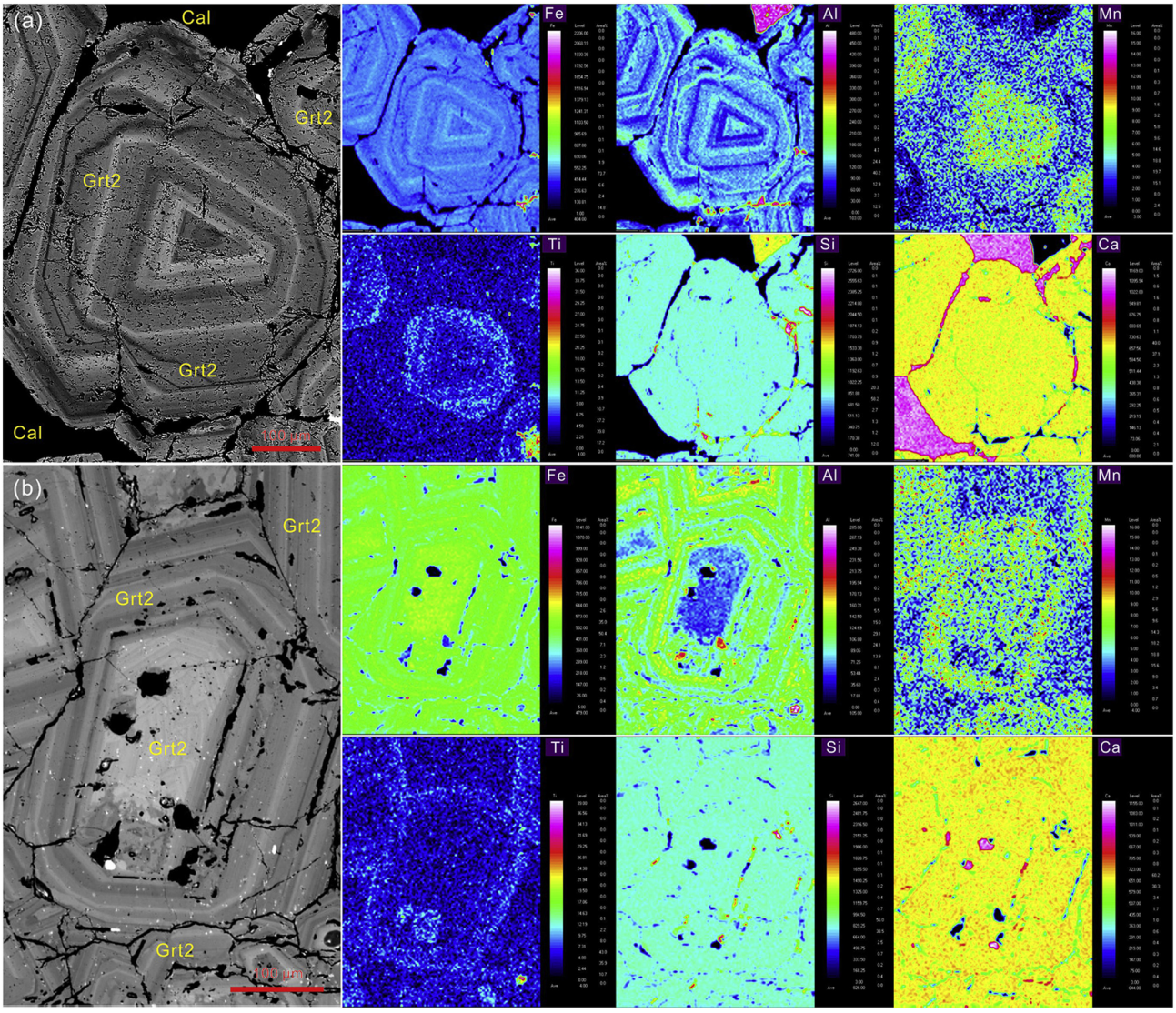

Fig. 4. Major elements EMPA mapping of Garnet2 at Tonglvshan.

are flat and stable during the ablation (ESM 1 Fig. 2). This further indicates that the distributions of U and other elements are homogeneous and short of the U-rich mineral inclusions in the selected grandite garnet at Tonglvshan.

The incorporation of U into the garnet is mainly controlled by: (1) substitution of divalent cations (Ca^{2+}, Mg^{2+}, Mn^{2+}, or Fe^{2+}) in the dodecahedral position; (2) substitution of REE, especially HREE in the eight-fold coordination site with similar ion radius; and (3) surface sorption during the growth of crystal (Jamtveit and Hervig, 1994; Smith et al., 2004; Gaspar et al., 2008; Dziggel et al., 2009). On the basis of similar ionic radius and charge balance ($[U^{4+}]^{VIII} + 2[Fe^{3+}, Al^{3+}]^{IV} - [Ca^{2+}]^{VIII} + 2[Si^{4+}]^{IV}$) (Gaspar et al., 2008), the incorporation of U in the Tonglvshan grandite garnet is probably depended on the coupled substitution of Ca^{2+} in the dodecahedral position and the substitution of Mg^{2+}, Mn^{2+} and Fe^{2+} are insignificant, due to their lower contents and poor correlation with U in the grandite garnets (ESM 2 and 3). The positive correlation between U and total REE (Fig. 7a) implies a similar ion substitution mechanism in an eight-fold coordination site within the Tonglvshan grandite garnet (Smith et al., 2004; Gaspar et al., 2008; Deng et al., 2017). However, this correlation is primarily reflected in LREE (Fig. 7b), but underperforming in HREE (Fig. 7c). The lack of positive correlation between U and LREE-HREE synchronously, suggesting that surface sorption was negligible for the incorporation of U into the Tonglvshan grandite garnet. Because surface sorption commonly causes U to correlate positively with both LREE and HREE in garnet (Jamtveit and Hervig, 1994; Smith et al., 2004).

At Tonglvshan, the magmatic-hydrothermal system is relatively oxidized. This is supported by the high zircon Ce^{4+}/Ce^{3+} ratios of the quartz monzodiorite (347–654) and quartz monzodiorite porphyry (348–1231) (Zhang et al., 2018a) and the estimated oxygen fugacity ($\log(fO_2)$ > NNN + 1) by the chemical composition of biotite in the quartz monzodiorite (Zhao et al., 2010). In this condition, high states of U ion (U^{5+}, U^{6+}) likely present in the crystal lattice of grandite garnet. Therefore, the oxidized magmatic-hydrothermal environment was more easily for U enrichment into grandite garnet.

Generally, crystal chemical arguments dictate U^{4+} merely fits dodecahedral sites, while U^{6+} occupies octahedral sites. In case of U^{5+} presents in octahedral sites, based on the first principle calculation, it needs to transfer its extra electron to neighboring tetrahedral Fe^{3+} (Rak et al., 2013; Guo et al., 2016). Therefore, the octahedral site may be more flexible to incorporate U with higher oxidation states (Guo et al., 2016). Compared with the reduced magmatic-hydrothermal system, the higher oxidized magmatic rocks and skarns may enrich U into the grandite garnet, such as the Ertsberg diorite and the related Big Gossan Cu—Au skarn deposit (Indonesia) with U concentration up to 200 ppm in the grandite garnet (Wafforn et al., 2018).

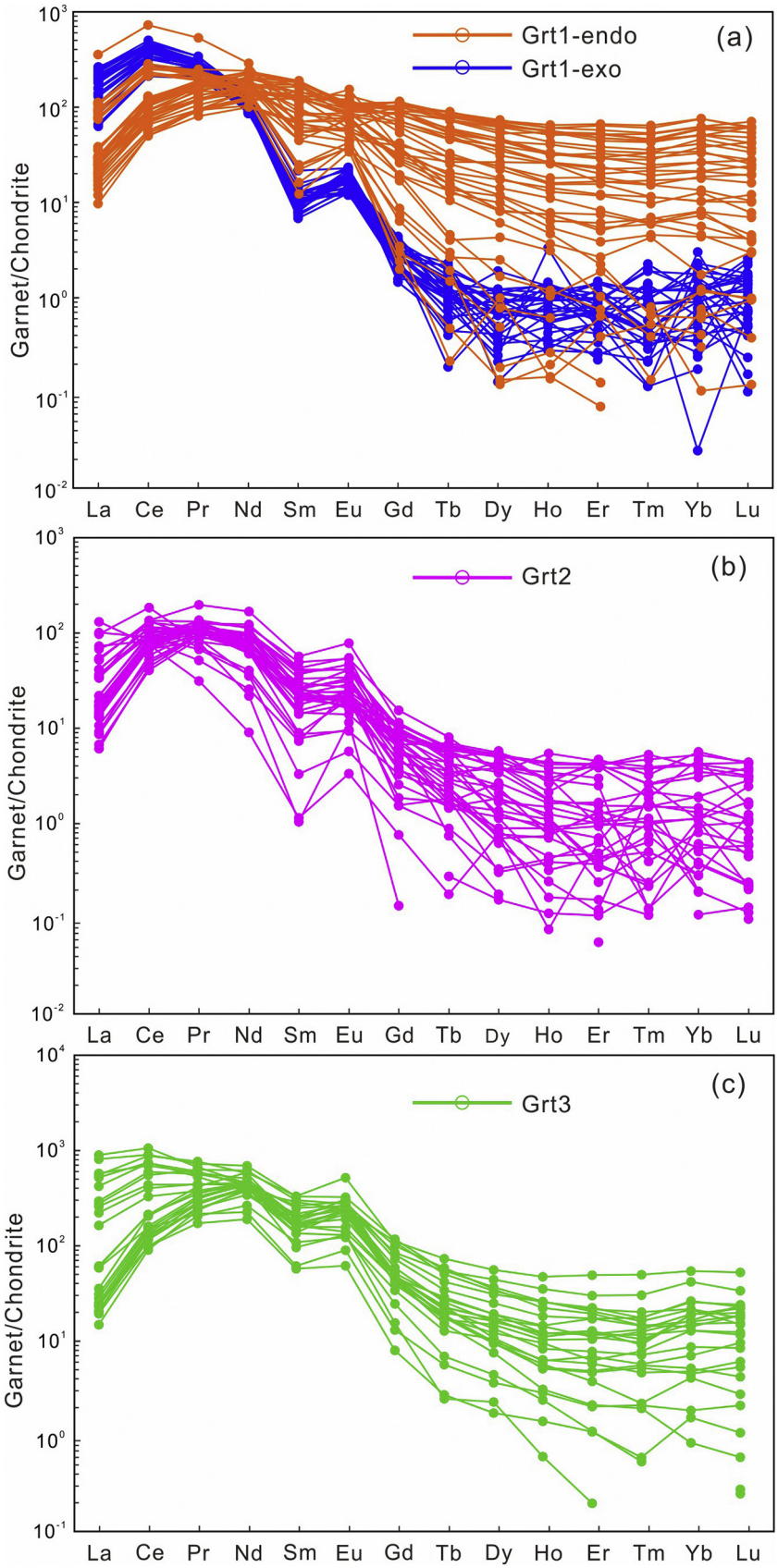

Fig. 5. Chondrite-normalized REE patterns of garnet in the Tonglvshan Cu-Fe-Au skarn deposit. Data sources: Chondrites (Boynton, 1984).

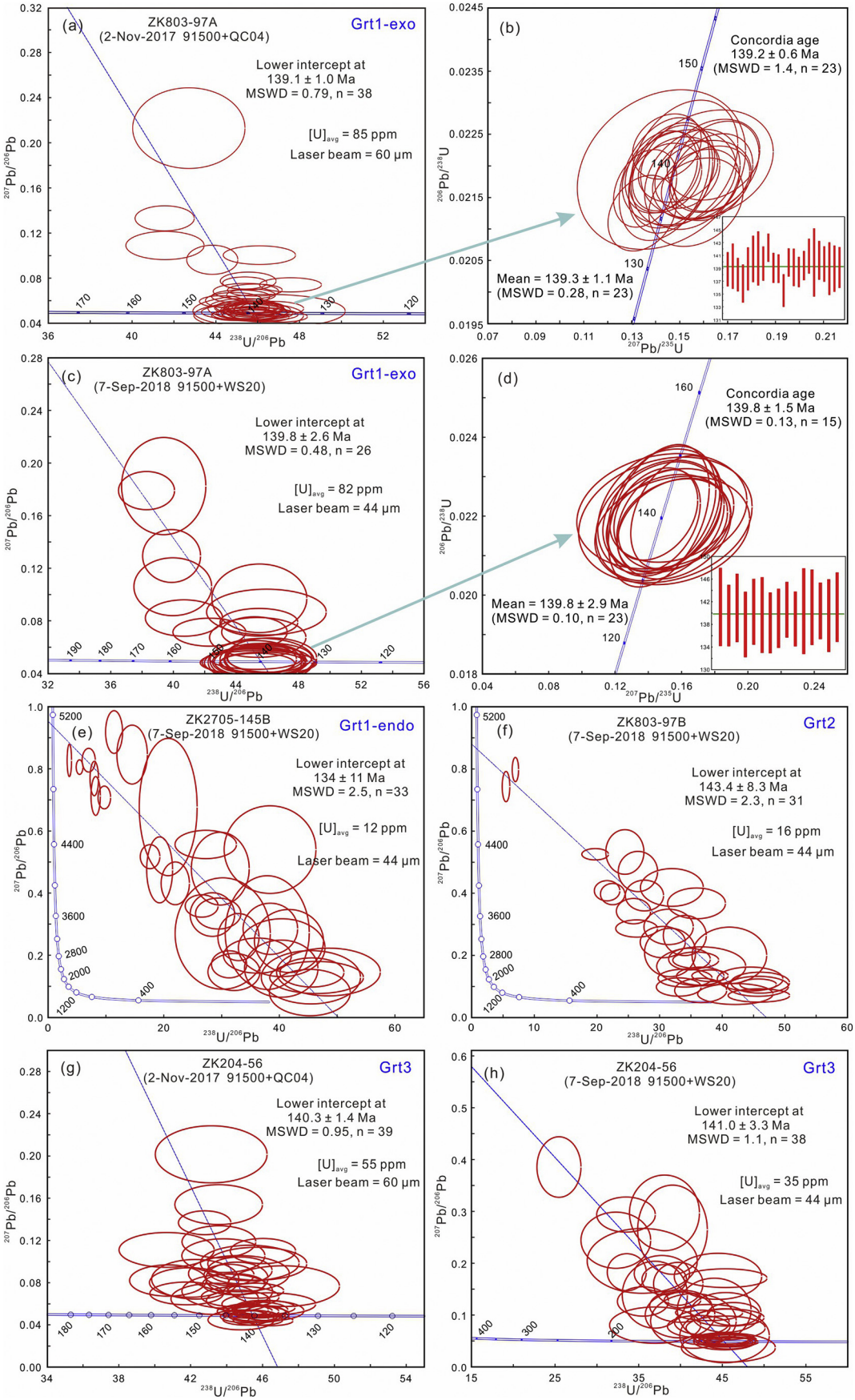

Fig. 6. Garnet U—Pb Tera-Wasserburg concordia and $^{207}Pb/^{235}U$-$^{206}Pb/^{238}U$ concordia diagrams and weighted mean $^{206}Pb/^{238}U$ ages for the different generations of garnet at Tonglvshan.

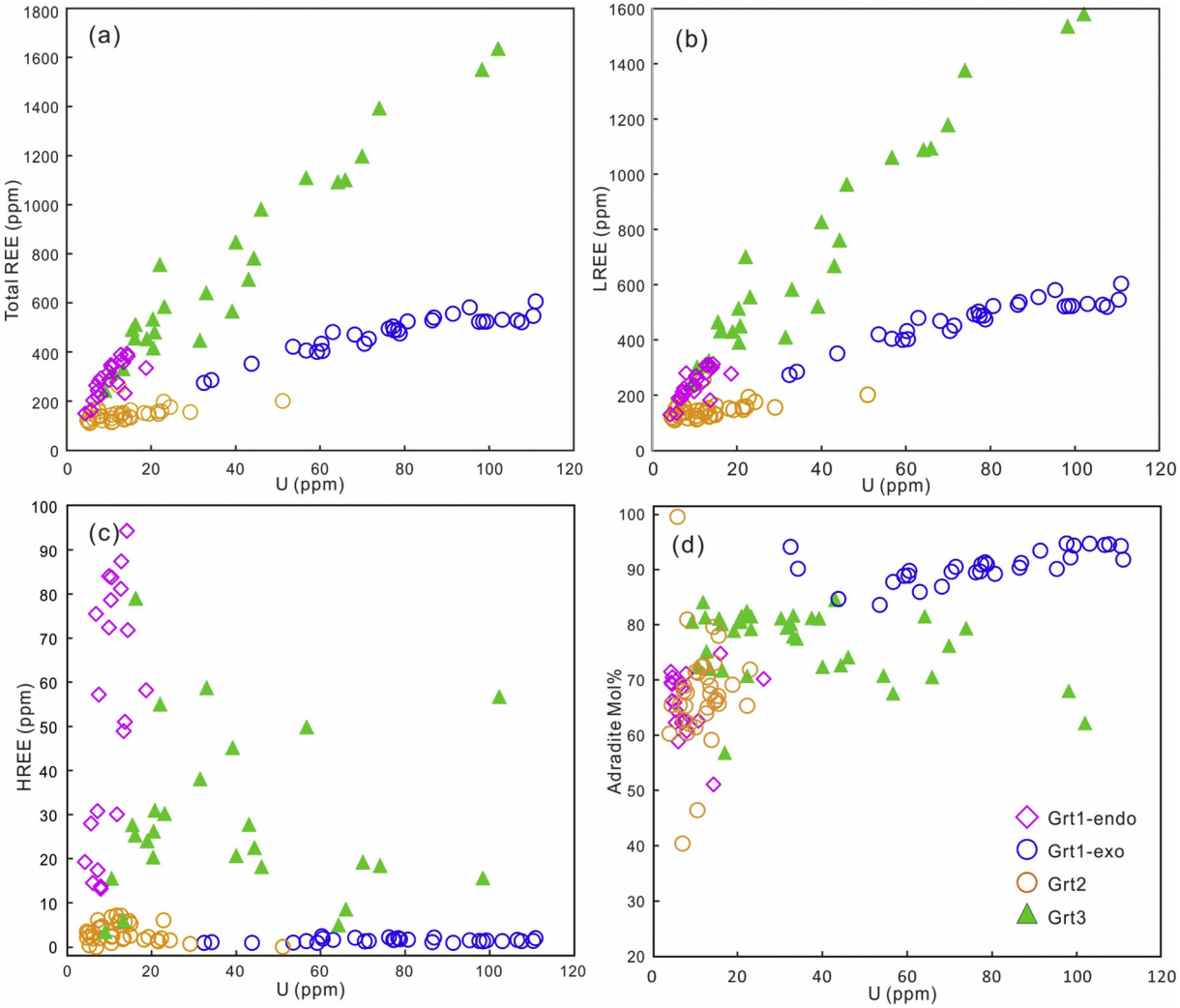

Fig. 7. Diagrams showing (a) U vs. total REE; (b) U vs. LREE; (c) U vs. HREE; and (d) U vs. andradite Mol% of the Tonglvshan garnet.

Several case studies and statistical analysis show that there is a common positive correlation between U concentration and andradite Mol% (Smith et al., 2004; Deng et al., 2017; Gevedon et al., 2018). At Tonglvshan, on the whole, high U contents show a relatively correspondence with high molar percentage of andradite (Fig. 7d). However, each generation of garnet shows striking difference of U concentration and andradite Mol% (Fig. 7d). In the core area of isotropic Grt1-exo, there is an obviously positive correlation between U concentration and andradite Mol% (Figs. 7d, 8a), but in the rim of Grt1-exo and the peripheral anisotropic Grt2 with elemental oscillatory zoning area, the concentration of U shows significantly decreasing with poor correlation of andradite Mol% (Figs. 7d, 8a, b). In the endoskarn zone, Grt1-edno also show monotonously low U concentration (Fig. 7d; ESM 4 Table 3). For the last generational garnet of Grt3, U concentrations are elevated and change dramatically with no obvious correlation between U concentration and andradite Mol% (Figs. 7d, 8c; ESM 4 Table 3). Therefore, it can be speculated that the incorporation of U into grandite garnet was not only influenced by the molar percentage of andradite, but may be also effected by the structure, paragenetic/metasomatic relationship of minerals and redox state. Moreover, the local buffering (wall rocks) and external buffering (fluids composition, P-T) conditions may also influenced the incorporation of U into grandite garnet. The grandite garnet was more easily to be enriched in U and obtain the high-precision concordia U—Pb ages with higher andradite Mol%, euhedral and larger crystal and high oxidized growth environment.

6.2. Evaluation of matrix effect

Various degrees of matrix effect often occurs in different minerals during LA-ICP-MS U—Pb isotopic analyses (e.g., Black et al., 2004; Liu et al., 2011). In order to avoid matrix effect, the same type of minerals was often used as the standard minerals. But for some low-U minerals with no suitable standards, such as xenotime, garnet and apatite etc., other appropriate minerals (e.g., zircon) can be selected (Deng et al., 2017; Li et al., 2018a). In some cases, an exorbitant laser energy density will reduce the accuracy due to the higher laser energy density could produce the larger aerosol particle size, which is harmful for the aerosol particle transportation and particle ionization in the ICP (Liu et al., 2011). In order to avoid large errors, similar to zircon U—Pb dating, in this study, we use a relatively lower laser energy density of 5 J/cm^2.

For the low-U minerals, in most instances, a larger spot size will obtain higher values of CPS (counts per second) and better accuracy (Wafforn et al., 2018). But in another case, the obtained U—Pb ages by LA-ICP-MS will decrease gradually with elevated beam spot size (Liu et al., 2011). In this study, we found that larger spot size (~60 μm) will make the lower errors of U—Pb isotopic data with slightly younger ages (Fig. 6a to d, g, h). Although there are several reported standard garnets, such as WS20 (Yang et al., 2018), QC04 (Deng et al., 2017) and OH-1 that close to Willsboro garnet and has similar U—Pb ages (Seman et al., 2017) in the laboratory of KLMRCE-SYU, the concordant $^{206}Pb/^{238}U$ ages was hardly to acquire because they are heterogeneous

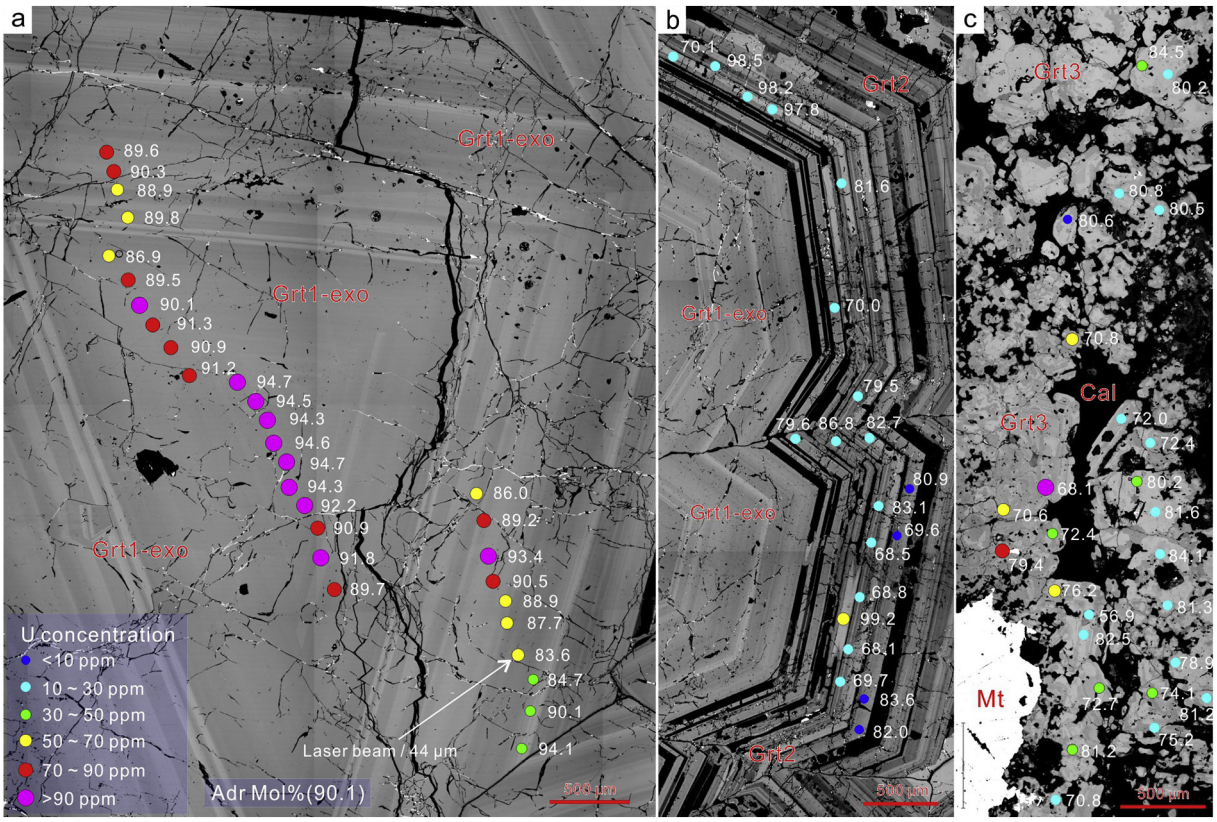

Fig. 8. Combined backscatter electron (BSE) micrograph images showing the location of laser beam spots on the polished thin section of garnet. Each spot is color coded based on the measured U concentration and corresponding andradite Mol%. (a) sample of ZK803-97A (Grt1-exo); (b) sample of ZK803-97B (Grt2); (c) sample of ZK204–56 (Grt3).

with variable common Pb contents. Some reported case studies show that the zircon standard (91500 and GJ-1), similar to Willsboro garnet (Seman et al., 2017), can effectively correct the U—Pb isotope fractionation and mass discrimination of garnet samples (Deng et al., 2017; Wafforn et al., 2018; Li et al., 2018a; Zhang et al., 2018b). For the Tonglvshan garnet, we selected QC04 and WS20 as the second garnet standard to monitor the garnet dating at different times. The monitoring analysis results as mentioned above also indicate that the obtained garnet U—Pb isotopic ages are credible.

These above facts indicate no distinct matrix effect between zircon 91,500 and the grandite garnet samples in the Tonglvshan Cu-Fe-Au skarn deposit. However, for more accurate, a matrix-matched external garnet standard with high CPS and neglectable common Pb contents might be still necessary for LA-ICP-MS U—Pb dating of garnet samples. Fortunately, in this study, for the selected sample spots of ZK803-97A with high U concentration, we firstly obtained the concordia garnet $^{206}Pb/^{238}U$ ages in skarn system. This result will provide a potential garnet U—Pb isotopic dating standard for the future study.

6.3. Timing and duration of the Tonglvshan skarn mineralization

In the past decade, multiple isotope dating methods have been applied to date the timing of the Tonglvshan Cu-Fe-Au mineralization (Li et al., 2010, 2014; Xie et al., 2011). One of the most used methods was $^{40}Ar—^{39}Ar$ geochronology of phlogopite that formed in the retrograde alteration stage (stage II) with Fe mineralization. However, unfortunately, total reported eleven $^{40}Ar—^{39}Ar$ plateau ages of phlogopite are discrepant, ranging from 148 to 136 Ma (Fig. 9; Xie et al., 2011; Li et al., 2014). In addition, Li et al. (2010) reported two titanite $^{206}Pb/^{238}U$ weighted mean ages of 135.9 ± 1.3 Ma (MSWD = 0.30; n = 14) and 121.5 ± 1.3 Ma (MSWD = 1.3; n = 12) in the Tonglvshan Cu-Fe-Au deposit. Xie et al. (2011) reported a molybdenite Re—Os isochron age (137 ± 2.4 Ma; MSWD = 1.3; n = 5) from the quartz-sulfide stage (stage IV) with Cu—Au mineralization.

Combined with the published ages of the Tonglvshan dioritic stock, some researchers suggested that there may exist multiple hydrothermal mineralization events (10–20 Myr) in the Tonglvshan ore district (Li et al., 2010, 2014). However, the mica Ar—Ar systematics with low closure temperature can easily be reset by later thermo-tectonic events (Chiaradia et al., 2013; Li et al., 2018a). The reliability of titanite U—Pb ages are relatively higher, but in some cases, can also be influenced by the later hydrothermal alteration with a younger U—Pb isotopic age (Deng et al., 2015b). Thus, based on the above variable geochronology data with a wide range, it is difficult to constrain the timing and duration of the Tonglvshan Cu-Fe-Au mineralization.

In this study, accurate LA-ICP-MS U—Pb dating on two grandite garnet samples from the pre-ore prograde skarn alteration (stage I; Grt1-exo) and Cu-Au-sulfide to post-ore carbonate stage (stage IV to V; Grt3) in the Tonglvshan Cu-Fe-Au deposit, yielded a precision concordia $^{206}Pb/^{238}U$ ages of 139.2 ± 0.6 Ma (2σ, MSWD = 1.4) and a lower intercept $^{206}Pb/^{238}U$ age of 140.3 ± 1.4 Ma (2σ, MSWD = 0.95), respectively (Fig. 6b, g). These ages are consistent with the majority of published high-precision zircon U—Pb ages (140–142 Ma) for the quartz monzodiorite and quartz monzodiorite porphyry at Tonglvshan (Fig. 9; Xie et al., 2011; Li et al., 2014; Zhang et al., 2018a), indicating a close genetic relationship between Tonglvshan dioritic stock and Cu-Fe-Au skarn mineralization. The age of 139–140 Ma can represent the onset of skarn alteration/mineralization, and indicate the duration of the metasomatic skarn mineralization event at Tonglvshan was relatively short-lived (< 1 Myr). Even taking into account the error range, it may be still <2.5 Myr. Our new results also provide a good example that a short-lived magmatic-hydrothermal process can account for the large-scale proximal Cu-polymetallic skarn mineralization.

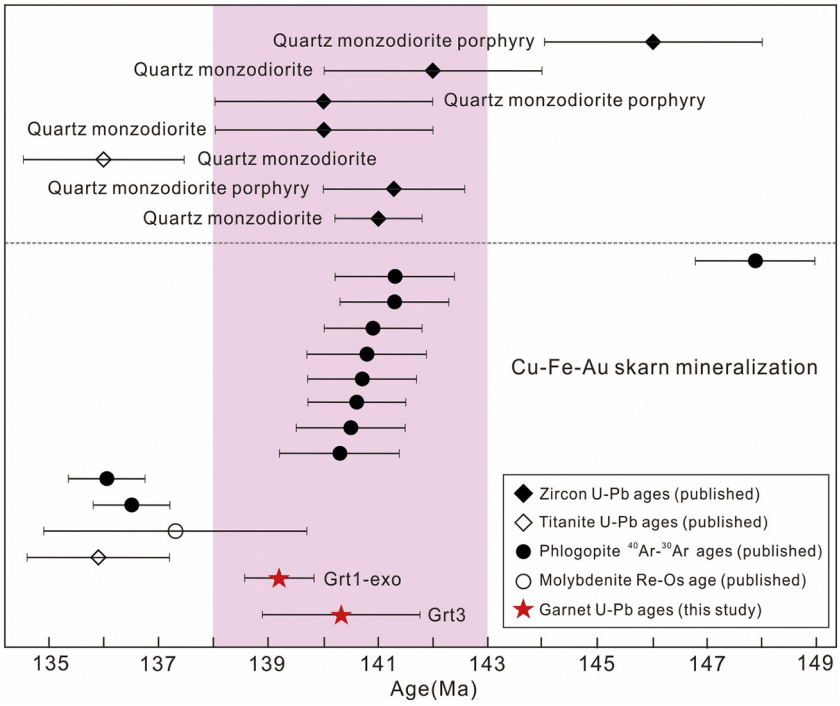

Fig. 9. Age spectra incorporating quartz monzodiorite and quartz monzodiorite porphyry and Cu-Fe-Au skarn mineralization at Tonglvshan deposit.

7. Conclusion

Three generation of garnets, including homogeneous Grt1-exo in the exoskarn zone and Grt1-endo in the endoskarn zone, oscillatory zoning Grt2 and vein-type Grt3 cutting magnetite ores were identified in the Tonglvshan skarn deposit. Uranium and common Pb contents are variable in each generational garnet and lead to different age errors. The precision grandite garnet concordia and lower intercept U—Pb ages from the Grt1-exo (139.2 ± 0.6 Ma) and Grt3 (140.3 ± 1.4 Ma) can be considered as the timing of Cu-Fe-Au skarn mineralization and indicate that the duration of metasomatic hydrothermal mineralization event at Tonglvshan <1 (or 2.5 considering errors) Myr. The grandite garnet with high andradite Mol%, euhedral and larger crystal and high oxidized growth environment was more easily to enrich in U and can obtain the high-precision concordia U—Pb ages.

Supplementary data to this article can be found online at https://doi.org/10.1016/j.gr.2019.04.003.

Acknowledgments

We would like to thank M. Santosh and two anonymous reviewers for their constructive comments that helped to significantly improve this manuscript. We also thank Dr. Dengfeng Li and Yu Fu and Miss Ying Liu (Lab engineer) at Guangdong Provincial Key Laboratory of Marine Resources and Coastal Engineering, School of Marine Sciences, Sun Yat-sen University in Guangzhou, China, for their technical assistance with LA-ICP-MS U—Pb and trace elements analysis of garnet. Thanks also to Dr. Changming Xing at Guangzhou Institute of Geochemistry, Chinese Academy of Sciences (CAS) in Guangzhou, China, for his technical assistance with EMP analysis. This study was financially supported by the Special Public Welfare Scientific Research fund Project by Ministry of Land and Resources, China (201511035) and Chinese National Science Fund (41725009).

Conflicts of interest

The authors declare no conflict of interest.

References

Black, L.P., Kamo, S.L., Allen, C.M., Davis, D.W., Aleinikoff, J.N., Valley, J.W., Mundil, R., Campbell, I.H., Korsch, R.J., Williams, I.S., Foudoulis, C., 2004. Improved $^{206}Pb/^{238}U$ microprobe geochronology by the monitoring of a trace-element-related matrix effect; SHRIMP, ID-TIMS, ELA-ICP-MS and oxygen isotope documentation for a series of zircon standards. Chemical Geology 205, 115–140.

Boynton, W.V., 1984. Cosmochemistry of the rare earth elements: meteorite studies. In: Henderson, P. (Ed.), Rare Earth Element Geochemistry. Elsevier, Amsterdam, pp. 63–114.

Burton, K.W., Kohn, M.J., Cohen, A.S., O'Nions, R., 1995. The relative diffusion of Pb, Nd, Sr and O in garnet. Earth and Planetary Science Letters 133, 199–211.

Chang, Z., Meinert, L.D., 2008. The empire Cu-Zn Mine, Idaho: exploration implications of unusual skarn features related to high fluorine activity. Economic Geology 103, 909–938.

Cheng, Y., Mao, J., Chang, Z., Pirajno, F., 2013. The origin of the world class tin-polymetallic deposits in the Gejiu district, SW China: Constraints from metal zoning characteristics and ^{40}Ar-^{39}Ar geochronology. Ore Geology Reviews 53, 50–62.

Chiaradia, M., Merino, D., Spikings, R., 2009. Rapid transition to long-lived deep crustal magmatic maturation and the formation of giant porphyry-related mineralization (Yanacocha, Peru). Earth and Planetary Science Letters 288, 505–515.

Chiaradia, M., Schaltegger, U., RICHARD Spikings, R., Wotzlaw, J.F., Ovtcharova, M., 2013. How accurately can we date the duration of magmatic-hydrothermal events in porphyry systems? Economic Geology 108, 565–584.

Deng, X.D., Li, J.W., Wen, G., 2015a. U-Pb Geochronology of Hydrothermal Zircons from the Early Cretaceous Iron Skarn Deposits in the Handan-Xingtai District, North China Craton. Economic Geology 110, 2159–2180.

Deng, X.D., Li, J.W., Zhou, M.F., Zhao, X.F., Yan, D.R., 2015b. In-situ LA-ICPMS trace elements and U-Pb analysis of titanite from the Mesozoic Ruanjiawan W-Cu-Mo skarn deposit, Daye district, China. Ore Geology Reviews 65, 990–1004.

Deng, X.D., Li, J.W., Luo, T., Wang, H.Q., 2017. Dating magmatic and hydrothermal processes using andradite-rich garnet U-Pb geochronometry. Contributions to Mineralogy and Petrology 172, 71.

Dewolf, C.P., Zeissler, C.J., Halliday, A.N., Mezger, K., Essene, E.J., 1996. The role of inclusions in U-Pb and Sm-Nd garnet geochronology: stepwise dissolution experiments and trace uranium mapping by fission track analysis. Geochimica et Cosmochimica Acta 60, 121–134.

Dziggel, A., Wulff, K., Kolb, J., Meyer, F.M., Lahaye, Y., 2009. Significance of oscillatory and bell-shaped growth zoning in hydrothermal garnet: evidence from the Navachab gold deposit, Namibia. Chemical Geology 262, 262–276.

Fang, J., Zhang, L., Chen, H., Zheng, Y., Li, D., Wang, C., Shen, D., 2018. Genesis of the Weibao banded skarn Pb-Zn deposit, Qimantagh, Xinjiang: Insights from skarn mineralogy and muscovite ^{40}Ar-^{39}Ar dating. Ore Geology Reviews 100, 483–503.

Fu, Y., Sun, X., Lin, H., Zhou, H., Li, X., Ouyang, X., Jiang, L., Shi, G., Liang, Y., 2015. Geochronology of the giant Beiya gold-polymetallic deposit in Yunnan Province, Southwest China and its relationship with the petrogenesis of alkaline porphyry. Ore Geology Reviews 71, 138–149.

Gaspar, M., Knaack, C., Meinert, L.D., Moretti, R., 2008. REE in skarn systems: a LA-ICP-MS study of garnets from the Crown Jewel gold deposit. Geochimica et Cosmochimica Acta 72, 185–205.

Gevedon, M., Seman, S., Barnes, J.D., Lackey, J.S., Stockli, D.F., 2018. Unraveling histories of hydrothermal systems via U-Pb laser ablation dating of skarn garnet. Earth and Planetary Science Letters 498, 237–246.
Grew, E.S., Locock, A.J., Mills, S.J., Galuskina, I.O., Galuskin, E.V., Halenius, U., 2013. Nomenclature of the garnet supergroup. American Mineralogist 98, 785–811.
Guo, X., Navrotsky, A., Kukkadapu, R.K., Engelhard, M.H., Lanzirotti, A., Newville, M., Ilton, E.S., Sutton, S.R., Xu, H., 2016. Structure and thermodynamics of uranium-containing iron garnets. Geochimica et Cosmochimica Acta 189, 269–281.
Jamtveit, B., Hervig, R.L., 1994. Constraints on transport and kinetics in hydrothermal systems from zoned garnet crystals. Science 263, 505.
Li, J.W., Deng, X.D., Zhou, M.F., Liu, Y.S., Zhao, X.F., Guo, J.L., 2010. Laser ablation ICP-MS titanite U-Th-Pb dating of hydrothermal ore deposits: a case study of the Tonglushan Cu-Fe-Au skarn deposit, SE Hubei Province, China. Chemical Geology 270, 56–67.
Li, J.W., Vasconcelos, P.M., Zhou, M.F., Deng, X.D., Cohen, B., Bi, S.J., Zhao, X.F., Selby, D., 2014. Longevity of magmatic-hydrothermal systems in the Daye Cu-Fe-Au District, eastern China with implications for mineral exploration. Ore Geology Reviews 57, 375–392.
Li, D., Fu, Y., Sun, X., 2018a. Onset and duration of Zn-Pb mineralization in the Talate Pb-Zn (-Fe) skarn deposit, NW China: Constraints from spessartine U-Pb dating. Gondwana Research 63, 117–128.
Li, D.F., Chen, H.Y., Hollings, P., Zhang, L., Sun, X.M., Zheng, Y., Xia, X.P., Xiao, B., Wang, C.M., Fang, J., 2018b. Trace element geochemistry of magnetite: Implications for ore genesis of the Talate skarn Pb-Zn (-Fe) deposit, Altay, NW China. Ore Geology Reviews 100, 471–482.
Li, Y., Selby, D., Li, X.H., Ottley, C.J., 2018c. Multisourced metals enriched by magmatic-hydrothermal fluids in stratabound deposits of the Middle-Lower Yangtze River metallogenic belt, China. Geology 46, 391–394.
Lima, S.M., Corfu, F., Neiva, A.M.R., Ramos, J.M.F., 2012. U-Pb ID-TIMS dating applied to U-rich inclusions in garnet. American Mineralogist 97, 800–806.
Liu, Y., Hu, Z., Zong, K., Gao, C., Gao, S., Xu, J., Chen, H., 2010. Reappraisement and refinement of zircon U-Pb isotope and trace element analyses by LA-ICP-MS. Chinese Science Bulletin 55, 1535–1546.
Liu, Z., Wu, F., Guo, C., Zhao, Z., Yang, J., Sun, J., 2011. In situ U-Pb dating of xenotime by laser ablation (LA)-ICP-MS. Chinese Science Bulletin 56, 2948–2956.
Ludwig, K.R., 2003. User's Manual for Isoplot 3.0: A Geochronological Toolkit for Microsoft Excel. Special Publication 4. Berkeley Geochronology Center.
Mao, J., Xie, G., Duan, C., Pirajno, F., Ishiyama, D., Chen, Y., 2011. A tectono-genetic model for porphyry-skarn-stratabound Cu-Au-Mo-Fe and magnetite-apatite deposits along the Middle–Lower Yangtze River Valley, Eastern China. Ore Geology Reviews 43, 294–314.
Meinert, L.D., Hedenquist, J.W., Satoh, H., Matsuhisa, Y., 2003. Formation of Anhydrous and Hydrous Skarn in Cu-Au Ore Deposits by Magmatic Fluids. Economic Geology 98, 147–156.
Meinert, L.D., Dipple, G.M., Nicolescu, S., 2005. World Skarn Deposits. Economic Geology, Economic Geology 100th Anniversary. pp. 299–336.
Mezger, K., Hanson, G.N., Bohlen, S.R., 1989. U-Pb systematics of garnet: dating the growth of garnet in the late Archean Pikwitonei granulite domain at Cauchon and Natawahunan Lakes, Manitoba, Canada. Contributions to Mineralogy and Petrology 101, 136–148.
Mezger, K., Rawnsley, S.R., Bohlen, S.R., Hanson, G.N., 1991. U-Pb garnet, sphene, monazite, and rutile ages: implications for the duration of high-grade metamorphism and cooling histories, Adirondack Mts., New York. Journal of Petrology 99, 415–428.
Nokleberg, W.J., 1981. Geologic setting, petrology, and geochemistry of zoned tungsten-bearing skarns at the Strawberry Mine, central Sierra Nevada, California. Economic Geology 76, 111–133.
Rak, Z., Ewing, R.C., Becker, U., 2013. Electronic structure and thermodynamic stability of uranium-doped yttrium iron garnet. Journal of Physics. Condensed Matter 25, 495–502.
Salnikova, E.B., Stifeeva, M.V., Chakhmouradian, A.R., Glebovitsky, V.A., Reguir, E.P., 2018. The U-Pb System in Schorlomite from Calcite-Amphobole-Pyroxene Pegmatite of the Afrikanda Complex (Kola Peninsula). Doklady Earth Sciences 478, 443–446.
Seman, S., Stockli, D.F., McLean, N.M., 2017. U-Pb geochronology of grossular-andradite garnet. Chemical Geology 460, 106–116.
Smith, M.P., Henderson, P., Jeffries, T.E.R., Long, J., Williams, C.T., 2004. The rare earth elements and Uranium in Garnets from the Beinn an Dubhaich Aureole, Skye, Scotland, UK: Constraints on Processes in a Dynamic Hydrothermal System. Journal of Petrology 45, 457–484.
Tornos, F., Delgado, A., Casquet, C., Galindo, C., 2000. 300 Million years of episodic hydrothermal activity: stable isotope evidence from hydrothermal rocks of the Eastern Iberian Central System. Mineralium Deposita 35, 551–569.
Wafforn, S., Seman, S., Kyle, J.R., Stockli, D., Leys, C., Sonbait, D., Cloos, M., 2018. Andradite garnet U-Pb geochronology of the Big Gossan skarn, Ertsberg-Grasberg ming district, Indonesia. Economic Geology 113, 769–778.
Xie, G., Mao, J., Zhao, H., Wei, K., Jin, S., Pan, H., Ke, Y., 2011. Timing of skarn deposit formation of the Tonglushan ore district, southeastern Hubei Province, Middle-Lower Yangtze River Valley metallogenic belt and its implications. Ore Geology Reviews 43, 62–77.
Xie, G., Mao, J., Zhu, Q., Yao, L., Li, Y., Li, W., Zhao, H., 2015. Geochemical constraints on Cu-Fe and Fe skarn deposits in the Edong district, Middle-Lower Yangtze River metallogenic belt, China. Ore Geology Reviews 64, 425–444.
Yang, Y.H., Wu, F.Y., Yang, J.H., Mitchell, R.H., Zhao, Z.F., Xie, L.W., Huang, C., Ma, Q., Yang, M., Zhao, H., 2018. U-Pb age determination of schorlomite garnet by laser ablation inductively coupled plasma mass spectrometry. Journal of Analytical Atomic Spectrometry 33, 231–239.
Yuan, S., Peng, J., Hao, S., Li, H., Geng, J., Zhang, D., 2011. In situ LA-MC-ICP-MS and ID-TIMS U-Pb geochronology of cassiterite in the giant Furong tin deposit, Hunan Province, South China: new constraints on the timing of tin-polymetallic mineralization. Ore Geology Reviews 43, 235–242.
Zhang, R., Lehmann, B., Seltmann, R., Sun, W., Li, C., 2017a. Cassiterite U-Pb geochronology constrains magmatic-hydrothermal evolution in complex evolved granite systems: the classic Erzgebirge tin province (Saxony and Bohemia). Geology 45, 1095–1098.
Zhang, Y., Shao, Y.J., Wu, C.D., Chen, H.Y., 2017b. LA-ICP-MS trace element geochemistry of garnets: Constraints on hydrothermal fluid evolution and genesis of the Xinqiao Cu-S-Fe-Au deposit, eastern China. Ore Geology Reviews 86, 426–439.
Zhang, S.T., Chen, H.Y., Han, J.S., Zhang, Y., Chu, G.B., Wei, K.T., Zhao, Y.J., Cheng, J.M., Tian, J., 2018a. Geochronology, geochemistry, and mineralization of quartz monzodiorite and quartz monzodiorite porphyry in Tonglüshan Cu-Fe-Au deposit, Edongnan ore district, China. Geochimica 47 (3), 240–256 (in Chinese with English abstract).
Zhang, Y., Shao, Y.J., Zhang, R.Q., Li, D.F., Liu, Z.F., Chen, H.Y., 2018b. Dating ore deposit using Garnet U-Pb geochronology: example from the Xinqiao Cu-S-Fe-Au Deposit, Eastern China. Minerals 8, 1–19.
Zhao, H.J., Mao, J.W., Xiang, J.F., Zhou, Z.H., Wei, K.T., Ke, F.Y., 2010. Mineralogy and Sr-Nd-Pb isotopic compositions of quartz diorite in Tonglüshan deposit, Hubei Province. Acta Petrologica Sinica 26, 768–784 (in Chinese with English abstract).
Zhao, W.W., Zhou, M.F., Chen, W.T., 2016. Growth of hydrothermal baddeleyite and zircon in different stages of skarnization. American Mineralogist 101, 2689–2700.
Zhou, T., Wang, S., Fan, Y., Yuan, F., Zhang, D., White, N.C., 2015. A review of the intracontinental porphyry deposits in the Middle-Lower Yangtze River Valley metallogenic belt, Eastern China. Ore Geology Reviews 65, 433–456.